

LONGITUDINAL MEASUREMENT OF ANNULAR-RING COUPLED STRUCTURE LINAC IN J-PARC

T. Maruta*, Y. Liu, KEK / J-PARC, Tokai, Japan
A. Miura, JAEA / J-PARC, Tokai, Japan

Abstract

The measurement of the longitudinal specification is a good method to inspect the tuning accuracy of RF cavities, an RF amplitude and a driving phase. The J-PARC linac was conducted a large modification in year 2013 to recover the beam energy to the original design of 400 MeV. The main upgrade is the installation of annular-ring coupled structure (ACS) cavities at SDTL downstream. The 400 MeV acceleration is successfully realized on January 17, 2014, and then we measure the longitudinal specifications. In this paper, we discuss the measurement results.

INTRODUCTION

After the beam energy upgrade, the J-PARC linac is comprised from a 50 keV negative hydrogen (H^-) ion source (IS), a 3 MeV radio frequency quadrupole (RFQ), a 50 MeV drift tube linac (DTL), an 191 MeV separate-type DTL (SDTL) and a 400 MeV annular-ring coupled structure (ACS) linac [1] as shown in Fig.1. ACS is a variation of coupled cavity linac with emphasis on the axial symmetry of the RF field [2]. The RF frequency of ACS is 972 MHz which is threefold frequency jump from SDTL. The ACS downstream is a beam transport section (L3BT) to a 3 GeV rapid cycling synchrotron (RCS). L3BT consists of the straight section, the first arc section, the collimator section, the second arc section and the injection section. Two debuncher cavities are placed in L3BT. The first debuncher (DB1) is located in the straight section and it is for the correction of the momentum centroid jitter. The second one (DB2) is at the downstream of first arc section and it is for the optimization of the momentum spread at the RCS injection. There are three beam dumps for a beam commissioning of the linac alone. Each beam dump are branched from the middle of L3BT. Most downstream dump is the 100 degree beam dump (100BD) and it is branched from the second arc section.

The first beam commissioning after the ACS installation had been conducted on December to January. We successfully realized 400 MeV acceleration on January 17. Because it is first time to accelerate by ACS, we need to confirm the property of ACS and to estimate the RF tuning accuracy of cavities. It motivated us to measure the ACS longitudinal properties after the realization of 400 MeV acceleration.

SIMULATIONS

Longitudinal Acceptance

This acceptance is calculated by 3D particle-in-cell code, IMPACT [3]. In the simulation, the initial particles are

* tmaruta@post.j-parc.jp

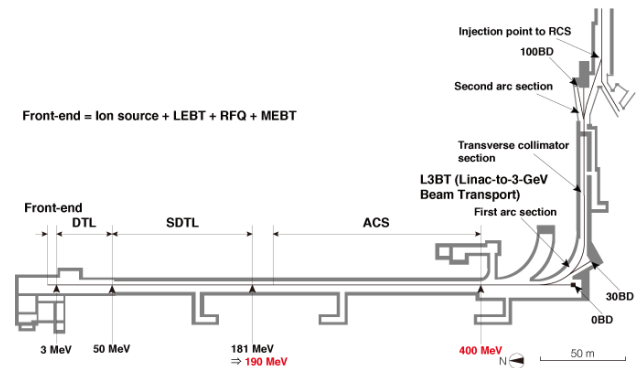


Figure 1: Outline of the J-PARC linac. In the initial stage, the linac had been operated at 181 MeV by the installation of IS to SDTL on the beam line as shown in black character. The ACS accelerator was installed at second stage to extend the beam energy to 400 MeV (red).

launched at the ACS entrance distributed over a sufficiently wide area to cover the entire acceptance in the longitudinal phase space. Then, we track these particles to the ACS exit without space charge. In the simulation, we adopt the Lorentz integrator with the step width of around $\beta\lambda/100$. Here, β and λ denote the particle velocity scaled by the speed of light and the RF wave length, respectively. No error is assumed. To eliminate the particles outside the bucket, we set an energy threshold at 396 MeV. We choose particles above the energy threshold at the ACS exit, and then find their initial positions at the ACS entrance to obtain the longitudinal acceptance. The area filled with pale blue dots in Fig. 2 shows the simulated acceptance for ACS. The horizontal axis in this figure is the beam injection phase to ACS with respect to the design synchronous phase ($\Delta\phi_s$). The vertical axis is the injection beam energy with respect to the design injection beam energy (ΔE). As seen in this figure, the acceptance is distributed from -30 to 60 deg in $\Delta\phi_s$ and from -2.7 to 2.4 MeV in ΔE , respectively.

Secondly, we evaluate the longitudinal beam distribution at the ACS entrance. The particle simulation is performed from the exit of RFQ to the entrance of ACS. The output distribution from PARMTEQM [4] is taken as the initial distribution [5]. In the simulation, we adopt the same integrator and the integration step width as the acceptance evaluation. However, the space charge effect is taken into account this time. We employ 100,000 macro-particles and $32 \times 32 \times 64$ meshes in the space-charge calculation, but no error is assumed. The longitudinal beam distribution at the ACS entrance is superimposed with red dots on the acceptance plot in Fig. 2.

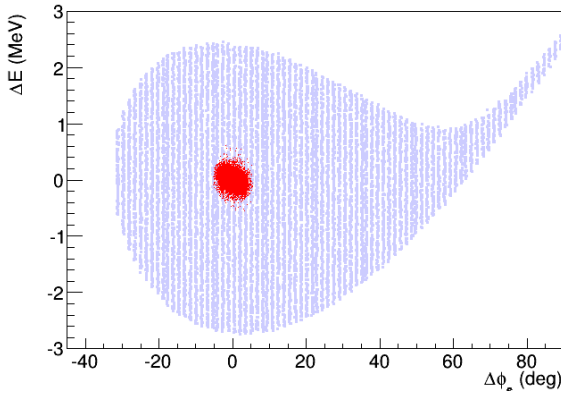


Figure 2: Longitudinal acceptance at the ACS entrance (pale blue points). Design beam distribution of the ACS entrance at peak current of 30 mA is also shown as red points.

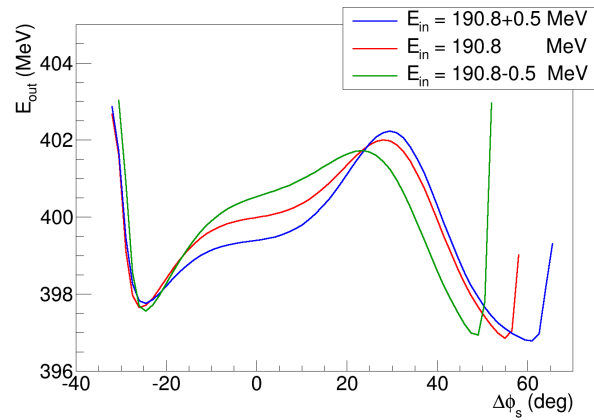


Figure 3: $\Delta\phi_s$ dependence of the output beam energy from ACS. In the simulation three injection energy is selected, 190.8 MeV (design, red) and 190.8±0.5 MeV (blue and red), respectively.

Output Beam Energy

If a macro particle is injected to ACS with an error ($\Delta\phi_s, \Delta E \neq 0$) but it is inside the acceptance, the particle is accelerated with circulating inside the acceptance to a counter-clockwise direction. Then, the beam is extracted with beam energy offset from the design. The amount of energy displacement depends on the injection phase and energy. The output beam energy is simulated by IMPACT when the injection phase and energy have a offset from the design. In the simulation, we choose three initial energies (E_{in}), 190.8 MeV (design) and 190.8±0.5 MeV. Initial particles are distributed over a sufficiently wide area on the phase direction. Then the particles are tracked at the exist of ACS without space charge. The output beam energy dependence on the initial phase is shown in Fig. 3. The horizontal axis in this figure is $\Delta\phi_s$, and the vertical axis is the output beam energy from ACS. The output energy varies from 396.5 to 403 MeV. In the negative side of $\Delta\phi_s$, energy is sharply increase by 5 MeV and its phase is almost same for three E_{in} s. Therefore, we can estimate the $\Delta\phi_s$ by checking the rising phase. Another point is a peak phase around 20 deg to 40 deg. This peak phase shifts to positive phase as the E_{in} being higher. Therefore, we can estimate the E_{in} from the distance of sharp rise phase at negative $\Delta\phi_s$ and the peak phase.

MEASUREMENTS

The experiment has been conducted at the peak current of 15 mA, which is the nominal peak current in the user operation. The beam destination is 100BD. Although the particles out of the acceptance are not accelerate and it causes the transverse mismatch, they can pass through the ACS section without any beam loss. If the beam pass though the first arc section, the section plays a role of a momentum collimation. Therefore we choose 100BD as a beam destination. The RF phase for the ACS cavities are varied while monitoring the beam transmission and the beam orbit downstream. The injection beam phase is shifted by changing the driving phase of all ACS cavities by the same amount.

Acceptance

The beam transmission is measured with current transformers (CT) which are designed to detect the peak current of beams. The average of two CT's in the MEBT2 section is taken as the injection beam current to ACS. Then, the average of two CT's at the first arc section downstream is taken as the output beam current. The beam transmission efficiency is defined as the ratio between these averages in this paper. Figure 4 shows the result of the transmission measurement. The phase of the injection beam is scanned from -45 deg to 80 deg with respect to the nominal phase setting. Assuming that the beam center is on the acceptance edge when the transmission is declined to 50 %, we can estimate the acceptance width in the phase direction. The experimental result in Fig. 4 indicates that the acceptance ranges from -32 deg to 60 deg in $\Delta\phi_s$. As already described above, the acceptance is distributed from -30 deg to 60 deg in the simulation. Therefore, the actual acceptance is wider than the design one by 2 deg.

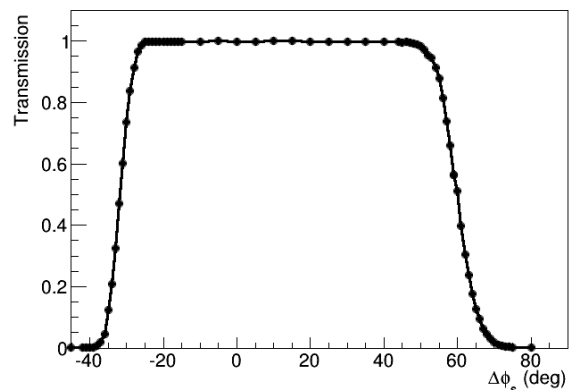


Figure 4: The result for the phase scan experiment. The dependence of the beam transmission on the injection beam phase are shown.

Output Beam Energy

In the middle of the first arc section, the dispersion function (η) is finite. The momentum variation causes the displacement of the beam orbit in the section. The beam orbit becomes a good probe to measure the momentum variation. We measure the beam position by beam position monitors (BPMs) in the section. Firstly, we evaluate the η of each BPM. The injection beam energy to the first arc section is shifted by changing the RF phase of DB1. We set the five momentum relative to the momentum at operation phase ($\Delta p/p$), -0.35% , -0.20% , 0.0% , 0.19% and 0.36% and beam position is measured. Then, the η is calculated by fitting the correlation of $\Delta p/p$ and the position displacement by a first order polynomial function. Red circles in Fig. 5 are results of the η measurement. The horizontal axis shows the distance from the L3BT entrance, and the vertical axis is η . The bottom figure of the histogram shows the lattice at the arc section. The green boxes show bending magnets and purple ones are quadrupole magnets, respectively. The measurements are well agreed to the design shown as a black line. We can see the threefold symmetric dispersion. The six BPMs are placed where η is around 0.51 m. Since the accuracy of the BPMs is 0.1 mm, the accuracy of $\Delta p/p$ measurement is expected to be 0.02 %.

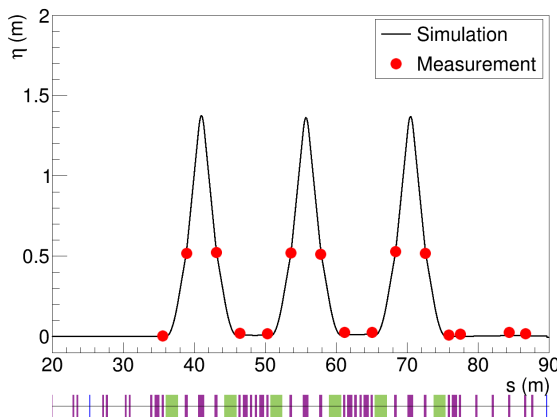


Figure 5: The result for the phase scan experiment. The dependence of the beam transmission on the injection beam phase are shown.

Figure 6 shows the measurement result of momentum variation. The phase of ACS injection beam is scanned from -30 deg to 55 deg with respect to the nominal phase setting. The beam position of the six BPMs is measured for each phase. Then, the $\Delta p/p$ is calculated from the horizontal displacement of beam position at $\Delta\phi_s = 0$ deg. The simulated $\Delta p/p$ curves are also plotted for a comparison. If the rising phase at negative edge of $\Delta\phi_s$, the measured curve and simulations are almost same behavior. Therefore, the injection phase is close to the design. Next, we compare the peak position around 20 deg to 40 deg. In the measurement, the peak position looks 25 deg. On the other hand, the peak position is 28 deg for $E_{in} = 190.8$ MeV and 23 deg

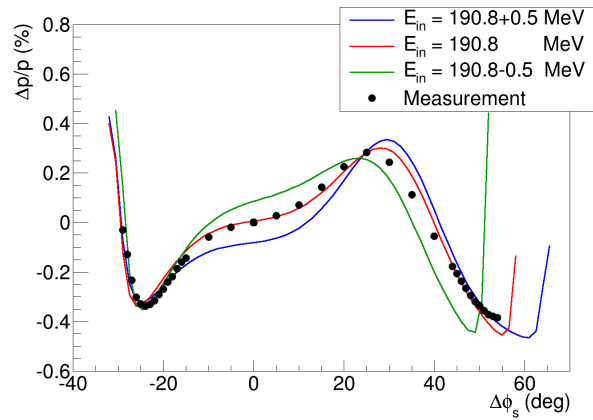


Figure 6: The result for the output beam momentum measurement from the displacement of beam position. The simulation results are also plotted for a comparison.

for $E_{in} = 190.8 + 0.5$ MeV. Therefore, the injection energy is considered a few hundred keV higher than the design.

SUMMARY

We measured longitudinal specifications of newly installed ACS accelerator, the acceptance width on the phase direction and output beam energy dependence on the injection beam energy. The acceptance is evaluated from the beam transmission to the first arc section downstream to be 92 deg. It is slightly larger than the design of 90 deg. The injection beam energy is estimated from the extraction beam energy with various injection phase. By comparing the extraction energy with the simulation, we evaluate that the injection beam energy is a few hundred keV higher than the design. Since the acceptance becomes wider as the injection energy being high as shown in Fig. 2, the wider acceptance could come from the higher injection energy.

REFERENCES

- [1] Y. Yamazaki ed., "Accelerator Technical Design Report for High-Intensity Proton Accelerator Project, J-PARC", KEK Report. 2002-013 (KEK, 2003).
- [2] H. Ao, et al., "First High-power Model of the Annular-ring Coupled Structure for Use in the Japan Proton Accelerator Research Complex Linac", Phys. Rev. ST Accel. Beams. 15 (2012), 011001.
- [3] J. Qiang, et al., "An Object-Oriented Parallel Particle-in-Cell Code for Beam Dynamics Simulation in Linear Accelerators", J. Comp. Phys. 163, 434 (2000).
- [4] K.R. Crandall, et al., "RFQ Design Codes", LANL Report, LA-UR-96-1836 (1996).
- [5] Y. Kondo, et al., "Particle Distributions at the Exit of the J-PARC RFQ", in Proceedings of LINAC2004, Lübeck, Germany, pp. 78-80.